RSC Chemical Biology

ROYAL SOCIETY OF CHEMISTRY

PAPER

View Article Online
View Journal

Cite this: DOI: 10.1039/d5cb00209e

A non-canonical function of RNF8 opposes TRAF6-mediated stabilization of HIF1α

Larissa Ringelstetter,†[a] Elisabeth Mersdorf-Weber,†[a] Kenji Schorpp‡[a] and Kamyar Hadian ‡*[ab]

Received 12th August 2025,
Accepted 13th May 2026

DOI: 10.1039/d5cb00209e

rsc.li/rsc-chembio

Ubiquitination is a central regulatory mechanism controlling protein stability and signaling in eukaryotic cells. The precise control of this machinery is crucial to avoid the development of diseases. Here, we identify a previously unrecognized interaction between the E3 ligase RNF8 and HIF1α, the oxygen-sensitive subunit of the hypoxia-inducible transcription factor HIF1. RNF8 antagonizes TRAF6-mediated stabilization of HIF1α under hypoxic conditions. Importantly, this regulatory effect is independent of the RNF8 E3 ligase activity but requires its forkhead-associated (FHA) domain. Yeast two-hybrid assays reveal an interaction between RNF8 FHA domain and the C-terminal transactivation domain (TAD) of HIF1α, despite the absence of a canonical FHA-binding motif in HIF1α. This interaction is maintained in a hydroxylation-deficient HIF1α mutant, indicating that prolyl hydroxylation is not required. Our findings suggest a non-canonical mode of FHA-dependent association by which RNF8 modulates HIF1α stability and downstream transcriptional control, with potential implications for hypoxia-driven signaling in triple-negative breast cancer.

Introduction

Ubiquitin-dependent signaling represents a major regulatory mechanism controlling protein turnover and cellular signaling pathways. E3 ubiquitin ligases play a central role in these processes by conferring substrate specificity to the ubiquitination machinery. The RING finger protein RNF8 is an E3 ubiquitin ligase best known for its role in the DNA damage response, where it orchestrates ubiquitin signaling at sites of DNA double-strand breaks.[1] RNF8 contains an N-terminal forkhead-associated (FHA) domain mediating phospho-dependent interactions,[2] a central coiled-coil region that promotes stable homodimerization, and a C-terminal RING domain responsible for recruitment of E2 ubiquitin-conjugating enzymes. Structural studies have demonstrated that RNF8 functions as a homodimer, engaging the heterodimeric E2 complex UBE2N/UBE2V2 to catalyze K63-linked ubiquitin chains.[3,4] This dimeric architecture is essential for its ubiquitin ligase activity and downstream signaling functions. Beyond genome maintenance, RNF8 has been implicated in various cellular processes,[5] including chromatin remodeling,[6] telomere maintenance and end protection,[7] and tumor progression.[8] Despite these advances, the full spectrum of RNF8 interaction partners and its functions outside the canonical DNA damage response remain incompletely understood.

HIF1α is a master regulator of the cellular response to hypoxia. Under normoxic conditions, hydroxylated HIF1α is ubiquitinated by the Von-Hippel-Lindau (VHL) E3 ligase complex and rapidly degraded *via* the proteasome.[9,10] In hypoxic conditions, this degradation pathway is inhibited, allowing HIF1α to accumulate, translocate to the nucleus, and form a transcriptionally active complex with HIF1β. This complex drives the expression of genes involved in angiogenesis, metabolism, and cell survival, such as VEGF and GLUT1.[11] Dysregulation of HIF1α is frequently observed in cancers, particularly in triple-negative breast cancer (TNBC), where it promotes glycolytic reprogramming, angiogenesis, metastasis, and therapy resistance.[12–14]

While the VHL pathway is well characterized, increasing evidence highlights the involvement of other E3 ligases in modulating HIF1α stability and activity. For instance, the RING-type E3 ligase TRAF6 stabilizes HIF1α under both normoxic and hypoxic conditions, enhancing its activity and downstream signaling.[15] Additionally, ligases such as Parkin have been shown to ubiquitinate HIF1α, targeting it for degradation, particularly under mitochondrial stress conditions.[16] Other E3 ligases, like MDM2 and SIAH2, influence HIF1α indirectly by targeting upstream regulators such as PHDs, thereby modulating its hydroxylation and subsequent degradation.[17,18] Despite these advances, the broader network of E3 ligases regulating

[a] *Helmholtz Zentrum München, Research Unit Signaling and Translation, Neuherberg, Germany. E-mail: kamyar.hadian@helmholtz-munich.de*
[b] *Comprehensive Pneumology Center (CPC-M), German Center for Lung Research (DZL), Munich, Germany*
† These authors contributed equally to this work.
‡ Co-senior authors.

HIF1α, particularly the dynamic interplay between stabilizing and destabilizing factors, remains poorly understood.

To gain a broader understanding of RNF8-dependent signaling networks, we performed a genome-wide yeast two-hybrid (Y2H) screen using RNF8 as bait. This unbiased approach identified HIF1α as a previously unrecognized RNF8-interacting protein. Given the central role of HIF1α in hypoxia signaling and tumor progression, we further investigated the functional relationship between RNF8, TRAF6, and HIF1α. Our results reveal a dynamic interplay between these proteins, in which RNF8 counteracts TRAF6-mediated stabilization of HIF1α and limits hypoxia-induced transcriptional responses. Because both TRAF6 and HIF1α are key regulators of hypoxia signaling and tumor progression in TNBC, these findings suggest a potential tumor-suppressive role for RNF8 and provide new insights into the regulation of HIF1α in cancer.

Experimental

Antibodies and expression vectors

The following primary antibodies were used for western blotting: anti-β-Actin (I-19, 1 : 1000, Santa Cruz), anti-GFP (B-2 1 : 1000, Santa Cruz), anti-HIF1α (ab16066 1 : 1000, Abcam), anti-RNF8 (B-2 1 : 1000, Santa Cruz), and anti-TRAF6 (EP591Y, 1 : 2000, Abcam), anti-H2A (ab18255 1 : 1000, Abcam), anti-GAPDH (sc-20357 1 : 10000, Santa Cruz). GFP-tagged expression constructs were cloned into pEGFP-C1 (Clontech), including RNF8 (WT, ΔFHA, I439D) and HIF1α (WT), and Flag-tagged variants cloned into a modified pEF4 vector,[19] including RNF8 (WT), TRAF6 (WT), and HIF1α (WT and deletion constructs). Yeast two-hybrid constructs were cloned into pGBKT7 or pGADT7 (Clontech, Matchmaker Gold System) as specified: RNF8 (WT, ΔFHA, ΔRING, FHA, RING), UBE2N, HIF1α (WT, TAD), SSR1, HERC2 (HECT), DNTTIP2, Cul4a, and Fam9B.

Yeast-two-hybrid (Y2H) assay

Protein–protein interactions were analyzed in living yeast cells using the Gal4-based Y2H system. By cloning the proteins of interest in the pGBKT7 (bait) or the pGADT7 (prey) vector, the bait protein is expressed as fusion to the Gal4 DNA binding domain (BD domain) while the prey protein is expressed as fusion to the Gal4 activating domain (AD domain). Y2H specific yeast strains (pJ69-7A, Y187, Y2HGold), which are auxotrophic for leucin, tryptophane, histidine and adenin were used, allowing the selection for successfully transformed cells on leucin and tryptophane lacking media (-Leu/-Trp) due to TRP1 and LEU2 markers at the respective plasmids. Only if bait and prey interact, Gal4 is able to transcribe the reporter gene *HIS3* and *Ade2* enabling cells to grow on histidine or adenine lacking media (-His, -Ade).

Transformation of yeast cells

For transformation, 1 μl plasmid DNA was added to 10 μl competent yeast and subsequently mixed with 360 μl PEG medium. After incubation for 30 min at room temperature (RT), cells were heated at 42 °C for 15 min. Yeast cells were pelleted by centrifugation (200×g, 5 min, RT) and resuspended in 100 μl sterile H_2O. The whole 100 μl were plated on -Leu/-Trp dropout plates to select for successful transformed yeast and incubated at 30 °C for 3–5 days. Positive protein–protein interactions were tested on -Leu/-Trp/-His or -Leu/-Trp/-Ade selection plates.

Yeast two-hybrid (Y2H) screening

A Y2H screen was performed using the Matchmaker Gold System (TaKaRa Bio, Clontech), following the manufacturer's instructions. The DNA sequence encoding amino acids 1–486 of RNF8 was amplified by PCR and cloned into the pGBKT7 vector, resulting in a bait construct (BD-RNF8). Screening was carried out against a normalized human cDNA library (Library-AD; Clontech), derived from a broad range of adult human tissues (male and female). This library has been normalized to reduce the representation of high-copy-number mRNAs and was pre-transformed into the Y187 (MATα) yeast strain by Clontech. To ensure the suitability of the bait construct, pGBKT7-RNF8 was tested for autoactivation and toxicity in the Y2HGold (MATa) reporter strain, using pGBKT7-empty as a negative control. As additional controls, pGADT7-UBE2N (positive control) and pGADT7-empty (negative control) were transformed into Y187 and used in parallel matings with Y2HGold. Mating was initiated by mixing equal amounts of freshly grown Y187 and Y2HGold cultures (~500 μl each) in YPD medium and incubating overnight at 30 °C with shaking (200 rpm). On the following day, a 1 : 100 dilution of the mating culture was plated on selective -Leu/-Trp, -Trp, and -Leu/-Trp/-His agar plates to select for diploid cells. Mating efficiency was calculated as the ratio of colony numbers on -Leu/-Trp/-His *versus* -Trp plates. A mating efficiency of 2–5% was considered acceptable, as recommended by the manufacturer. For the full-scale screen, 4–5 ml of a concentrated overnight culture of the bait strain (Y2HGold transformed with pGBKT7-RNF8, $>1 \times 10^8$ cells per ml) was mixed with 1 ml of the library strain (Y187 with Library-AD) in 45 ml YPD medium, and incubated for 24 h at 30 °C, 50 rpm. After mating, cells were pelleted (10 min, 1000× g, room temperature), resuspended in 10 ml fresh YPD medium, and plated onto 100 -Leu/-Trp/-His selective agar plates (100 μl per plate). After 5 days of incubation at 30 °C, ~1600 colonies were observed. All colonies were subsequently replated onto high-stringency selection plates (-Leu/-Trp/-His/-Ade) supplemented with X-α-Gal and Aureobasidin A. Plasmids from single colonies were isolated using the Easy Yeast Plasmid Isolation Kit (TaKaRa Bio, Clontech) and sent for sequencing.

Cultivation of human cell lines

This study did not involve human participants or primary human tissues. All experiments were performed using established human cell lines. MDA-MB-231 and HEK293T cells were obtained from ATCC (ATCC® HTB-26™ and ATCC® CRL-3216™, respectively). Therefore, ethical approval and informed consent were not required. All cell lines were maintained at 37 °C in a humidified atmosphere containing 5% CO_2 and cultured in

medium supplemented with 10% fetal bovine serum (FBS) and 1% penicillin–streptomycin. MDA-MB-231 cells were grown in Dulbecco's modified Eagle medium (DMEM) high glucose with GlutaMAX™, supplemented with 10% FBS, 1% penicillin–streptomycin, and 1% non-essential amino acids (NEAA). HEK293T cells were cultured in standard DMEM supplemented with 10% FBS and 1% penicillin–streptomycin. Cells were passaged when they reached approximately 90% confluence. For subculturing, cells were washed once with 1x PBS and detached using 2 ml of 0.5% Trypsin-EDTA. Trypsinization was stopped by adding 8 ml of complete growth medium, and cells were then resuspended, diluted, and seeded as required for further experiments.

Transfection of human cells

HEK293T and MDA-MB-231 cells were transfected using X-tremeGENE™ HP DNA Transfection Reagent (Roche) according to the manufacturer's protocol. For each transfection, DNA and transfection reagent were pre-incubated in Opti-MEM® reduced serum medium before being added to the cells. Cell number, dish format, and transfection mix varied depending on the downstream application, as summarized below:

- Co-IP assay: 2×10^6 cells in a 10 cm dish with 10 ml medium; transfection mix: 200 µl Opti-MEM + 4 µg total DNA + 10 µl transfection reagent
- Cell lysate preparation: 3×10^6 cells in a 10 cm dish with 10 ml medium; transfection mix as above
- qPCR analysis: 4×10^5 cells in a 6 cm dish with 3 ml medium; transfection mix: 200 µl Opti-MEM + 6 µg total DNA + 15 µl transfection reagent

In general, cells were seeded one day prior to transfection and harvested 24 hours after transfection. For experiments under hypoxic conditions, cells were transferred to low oxygen environments (0.1% O_2) 10 hours post transfection and incubated for an additional 24 hours. For hypoxia-mimetic conditions, cells were treated with 300 µM $CoCl_2$ or sterile water (control) 10 hours post transfection, followed by incubation for another 20 hours.

cDNA synthesis and quantitative real-time PCR (qRT-PCR)

Total RNA was reverse-transcribed into cDNA using the SuperScript™ III First-Strand Synthesis System (Thermo Fisher Scientific), following the manufacturer's instructions. Random hexamers provided with the kit were used as primers for reverse transcription. Quantitative real-time PCR was performed using the LightCycler® 480 (LC480) system in combination with the KAPA SYBR® Fast qPCR Kit (Roche). For each target gene, a specific primer pair was used, and expression levels were normalized to the housekeeping gene RPL27, which served as an internal control to account for differences in RNA input. The primer sequences used in this study were as follows:

HIF1α forward: 5′-CGT CGA AAA GAA AAG TCT CGA GAT-3′;
HIF1α reverse: 5′-AGG CCT TAT CAA GAT GCG AAC T-3′
VEGF forward: 5′-CTC TAC CTC CAC CAT GCC AAG T-3′;
VEGF reverse: 5′-GCT GCG CTG ATA GAC ATC CA-3′
Glut1 forward: 5′-GCG GGT TGT GCC ATA CTC AT-3′;
Glut1 reverse: 5′-ACT TCA AAG AAG GCC ACA AAG C-3′
RPL27 forward: 5′-TCG CCA AGA GAT CAA AGA TAA-3′;
RPL27 reverse: 5′-CTG AAG ACA TCC TTA TTG ACG-3′

Prior to amplification, the 96-well plate was sealed and centrifuged for 2 minutes at 200 × *g*. PCR reactions were run according to standard cycling conditions recommended by the manufacturer. To confirm amplification specificity, melting curve analysis was performed for each reaction. Relative gene expression levels were calculated using the ΔΔCp method, in which Cp values of the target genes were first normalized to RPL27 and then compared to the appropriate control sample. All experiments were conducted using at least three independent biological replicates, and data are presented as mean ± standard deviation (SD). Statistical analysis was carried out using GraphPad Prism, applying a two-tailed unpaired Student's *t*-test. A *p*-value of less than 0.05 was considered statistically significant ($p < 0.05$).

Co-Immunoprecipitation assays

For transient overexpression of proteins, 2×10^6 HEK293T cells were seeded in a 10 cm dish and transfected the following day with a total of 4 µg plasmid DNA (2 µg per construct) as described above. Twenty-four hours after transfection, cells were washed once with PBS, then lysed in 200 µl ice-cold RIPA buffer (10 mM Tris–HCl pH 7.5, 150 mM NaCl, 0.5 mM EDTA, 2.5 mM $MgCl_2$, 0.1% SDS, 1% Triton-X-100, 1% Deoxycholate, 1 mM PIC). Cells were scraped off the plate and lysed by repeated passage through a 26G needle to ensure efficient disruption. The lysate was rotated end-over-end at 4 °C for 30 minutes, and insoluble material was removed by centrifugation at 20 000 × *g* for 20 minutes at 4 °C. The supernatant was transferred to a fresh tube and diluted with 300 µl GFP-TRAP wash buffer (10 mM Tris-HCl pH 7.5, 150 mM NaCl, 0.5 mM EDTA). A 50 µl aliquot of this diluted lysate was mixed with 20 µl SDS loading buffer and used as the input control. The remaining supernatant was incubated with 20 µl pre-washed GFP-TRAP beads (washed 3× in 1 ml GFP-TRAP wash buffer, centrifuged at 2500 × *g* for 2 minutes at 4 °C) for 1 hour at 4 °C on a rotator. To isolate GFP-tagged proteins, samples were centrifuged at 2500 × *g* for 2 minutes, and the beads were washed three times with 1 ml GFP-TRAP wash buffer. After the final wash, all residual buffer was carefully removed, and proteins were eluted by adding 50 µl SDS loading buffer directly to the bead pellet. Both input samples and eluates were heated at 100 °C for 5 minutes, separated by SDS-PAGE, and analyzed by western blotting using specific antibodies.

Inducing hypoxia and hypoxia-mimicking conditions

To induce cellular hypoxia, HEK293T and MDA-MB-231 cells were cultured under 0.1% O_2 and 5% CO_2 for 24 hours using a hypoxia chamber (Baker & Ruskinn). For harvesting, cells were immediately transferred to ice upon removal from the chamber. All subsequent steps, including PBS washes and lysis, were performed rapidly to preserve hypoxia-related molecular signatures. To mimic hypoxic conditions chemically, cells were treated with 300 µM cobalt chloride ($CoCl_2$) for 20 hours. $CoCl_2$ powder was freshly dissolved in sterile H_2O. As a negative

control, cells were treated with H_2O alone. Cell number and well format varied depending on the specific assay.

siRNA and subcellular localization

RNF8 localization under hypoxia-mimicking conditions was assessed using $CoCl_2$ treatment and fractionation assays were performed to determine nuclear translocation. Therefore, 4 × 10^6 MDA-MB-231 cells were seeded in a 10 cm dish and hypoxic mimicking conditions (300 μM $CoCl_2$) were induced as indicated above. After 20 hours, cells were harvested on ice by trypsinization and collected in ice-cold DBPS. Cells were pelleted for 5 min, 4 °C at 250 g and subsequently washed three times with ice-cold DPBS. The cell pellet was then lysed by adding 300 μl REAP-lysis-buffer (1 × DBPS, 0,1% NP-40) and incubated 3 min on ice. After centrifugation for 5 min, 500 g, 4 °C, 100 μl of supernatant were boiled with 4 × Laemmli sample buffer as cytoplasmic fraction. The resulting nuclei pellet (= nuclear fraction) was subsequently washed 3 × with REAP buffer and the final nuclei pellet was boiled in 90 μl 2 × Laemmli sample buffer and sonified 3 ×, 5 s, amplitude = 80. Samples were separated by SDS-PAGE, proteins were analyzed by antibody detection on western blot membranes, and H2A (Nuclear) and GAPDH (Cytoplasmic) were used as quality controls for the indicated fractions.

For siRNA treatment, 2 × 10^6 MDA-MB-231 cells were seeded in a 10 cm dish and transfected the next day with 180 pmol of the indicated siRNAs using lipofectamine RNAiMAX (Thermo Fisher Scientific) according to manufacturer instructions. After 6 hours, medium was changed to regular DMEM and the following day, $CoCl_2$ was added for 20 hours and samples were prepared as described previously.

Results and discussion

Identification of RNF8-HIF1α Interaction

In this study, we aimed to uncover previously unknown interaction partners of RNF8 to gain deeper insights into its diverse biological functions. To this end, we performed a genome-wide yeast two-hybrid (Y2H) screen using full-length RNF8 as bait. The Y2H screen yielded 34 confirmed interaction partners (Fig. 1A and Fig. S1), which were ranked based on hit frequency (Fig. S2). Among the top-ranking hits was UBE2N, a well-established RNF8 interaction partner. The robust recovery of UBE2N in the screen is in line with previous structural and biochemical studies, demonstrating robust binding of RNF8 dimers to the UBE2N/UBE2V2 complex and thus serves as an internal positive control validating the reliability and specificity of our screening approach.

To gain a functional overview, we categorized the identified proteins using a color-coded scheme based on their most associated biological pathways (Fig. 1B). The interactors span a broad range of functional classes, including components of the ubiquitin system, DNA damage response, RNA processing, and chromatin-associated processes. Importantly, several of the identified proteins have previously been reported as RNF8 interaction partners in public databases and published studies, including HERC2, UBE2N, UBE2W, BCLAF1, PHAX, SSR1, FAM9B and DNTTIP2.[20–24] The re-identification of these known interactors underscores the robustness and specificity of the Y2H screening approach in this study. To refine our dataset, we excluded all hits that appeared fewer than three times in the screen (Fig. 1A and Fig. S2). This filtering step resulted in 13 candidate proteins, including the well-described RNF8-interactors HERC2 and UBE2N. However, it should be noted that several low-frequency hits were excluded by our selection criterion (*e.g.*, UBE2W) that have previously been reported as RNF8 interaction partners, indicating that biologically relevant interactions may also be present among less frequently recovered candidates. To prioritize candidates for further validation, we analyzed the expression levels of BD-RNF8 and all 13 AD-constructs by western blot (data not shown). Based on these data, we selected 8 promising candidates and cloned their full-length coding sequences into Y2H constructs for retesting. Using these constructs, we were able to confirm interactions for UBE2N, HIF1α, CUL4a and FAM9B (Fig. 1C). While the recovery of UBE2N and FAM9B is consistent with previously reported RNF8 interactions, CUL4A and HIF1α represent previously unrecognized candidate RNF8-interacting proteins. In contrast, several proteins identified in the initial screen, including HERC2, DNTTIP2, and SSR1, could not be confirmed under these retesting conditions. This likely reflects differences between the initial screening setup and full-length retesting, such as domain accessibility and protein expression.

Among the confirmed interactions, HIF1α emerged as a particularly interesting candidate due to its central role in hypoxia signaling and its critical contribution to tumor development and progression in multiple cancer types. The RNF8-HIF1α complex formation was robustly validated in the Y2H system using constructs expressing the full-length proteins (Fig. 1D). Importantly, the closely related E3 ligase RNF168 did not interact with HIF1α (Fig. 1D), suggesting a specific and previously unrecognized link between RNF8 and HIF1α.

Next, we further validated the association between RNF8 and HIF1α by co-immunoprecipitation (co-IP) followed by western blot analysis in HEK293T cells ectopically expressing flag-tagged RNF8 and GFP-tagged HIF1α. As shown in Fig. 1E, Flag-RNF8 specifically co-precipitated with GFP-HIF1α, but not with GFP alone, confirming the specificity of the interaction. Notably, repeating the co-IP experiment with reversed protein tags yielded the same result (Fig. 1F), further supporting the robust interaction between RNF8 and HIF1α. To determine whether RNF8 also interacts with endogenous HIF1α, we treated cells with $CoCl_2$, a hypoxia mimicking agent, to stabilize HIF1α protein levels and performed GFP-Trap pull-downs using GFP-RNF8. Under these conditions, we were able to detect endogenous HIF1α in complex with GFP-RNF8, thereby supporting the physiological relevance of the interaction (Fig. 1G). Together, these results confirm the interaction observed in the Y2H screen. While a recent proteomics-based study from 2022 generated a high-confidence reference map of the RNF8 interactome in cancer cells *via* LC-MS and *in vitro* validation,[23] it did not identify

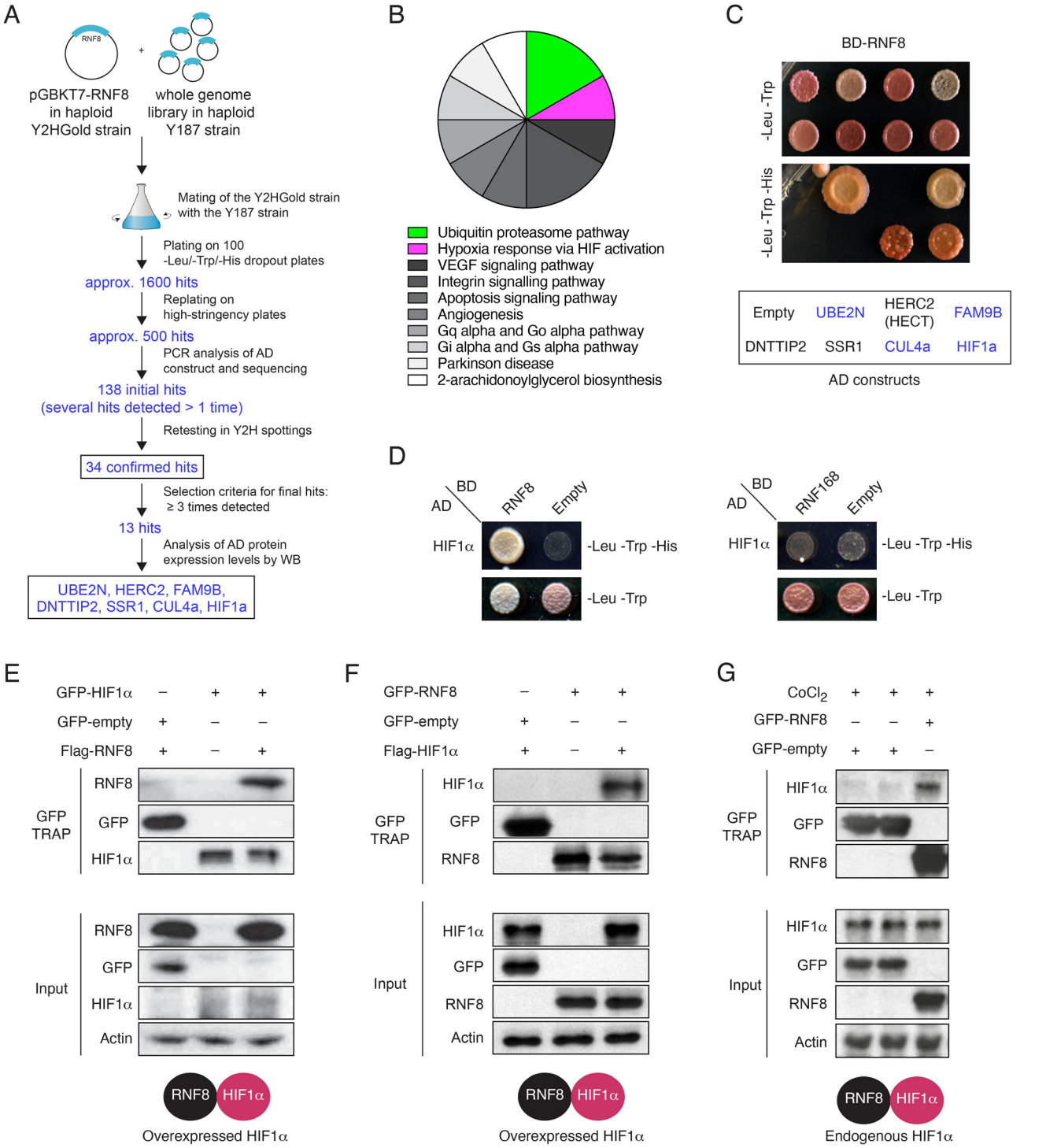

Fig. 1 RNF8 interacts with HIF1α in yeast and mammalian cells. (A) Scheme of the RNF8 Y2H screen representing the hit selection and hit verification strategy. (B) Functional categorization of 34 confirmed Y2H hits based on GO annotations. (C) Validation of selected full-length Y2H interactors with RNF8 in direct pairwise assays. (D) Confirmation of RNF8-HIF1α interaction using RNF8 and RNF168 (negative control). (E) and (F) Co-immunoprecipitation (co-IP) of GFP-HIF1α and Flag-RNF8 (E) or reciprocal constructs (F) in HEK293T cells. (G) GFP-RNF8 co-precipitates endogenous HIF1α following $CoCl_2$ treatment in HEK293T cells.

HIF1α as an RNF8 binding partner. This absence is likely due to the low expression and rapid degradation of HIF1α under normoxic conditions, which typically limits its detection in proteomic screens. In contrast, our Y2H screen was performed in yeast, where HIF1α is stably expressed and not subject to oxygen-dependent degradation. This strategy successfully revealed the

RNF8-HIF1α interaction, highlighting a key advantage of Y2H approaches for capturing low-abundance or context-specific interactions.

Mapping the interaction domains within RNF8 and HIF1α

In the next step, we sought to determine which domains of the two proteins mediate this interaction. To this end, we generated a series of truncation constructs for both RNF8 and HIF1α and performed domain-mapping studies using Y2H assays. All constructs are summarized in Fig. 2A. Interestingly, we found that HIF1α selectively interacts with the N-terminal FHA domain of RNF8 and not with C-terminal RING domain, the E2 enzyme binding site (Fig. 2A). The FHA domain of RNF8 is a phospho-protein binding module and is important for its subcellular localization.[2] HIF1α WT as well as the C-terminal TAD domain of HIF1α interacted with RNF8 WT, RNF8 (FHA) as well as the RNF8 ΔRING truncation in Y2H (Fig. 2B). Thus, the interaction of RNF8 with HIF1α seems to be independent of its RING E3 ligase domain. To verify this finding in human cells we overexpressed HIF1α WT together with RNF8 WT, RNF8 ΔFHA and RNF8 I439D. I439D bears a point mutation in the RING domain of RNF8, causing its inactivation by abolishing complex formation with UBE2N (also known as Ubc13). HIF1α WT co-precipitated with RNF8 WT as well as its catalytically inactive variant RNF8 I439D. However, RNF8 lacking the FHA domain (ΔFHA) did not bind HIF1α WT (Fig. 2C-D). GFP-empty served as a negative control and did not co-precipitate with either form of HIF1α (Fig. 2D). These data indicate an interaction between the HIF1α TAD and the RNF8 FHA domains. Our findings compare well with the characteristics of the FHA domain, which generally mediates protein–protein interactions.[25,26] The FHA domain of RNF8 recognizes a short amino acid sequence around a central phospho-Threonin (pThr), with either Tyr or Phe in the +3 position (pTxxY/F).[2] The strong selection for this motif is rather unique compared to other FHA domains for which X-ray crystal structures are available.[2,26,27] We were able to localize the pTxxY/F motif in HIF1α at three different sites, all in the N-terminal region (data not shown). However, this is rather inconclusive, since we show that RNF8 is able to interact with only the C-terminal TAD domain of HIF1α, which lacks all possible pTxxY/F interaction motifs. Noteworthy, there is a described phosphorylation site in the C-terminal TAD domain of HIF1α at T796.[28] It is not followed by Tyr or Phe in the +3 position, and is therefore not predicted as a RNF8 interaction motif, but could still govern the interaction

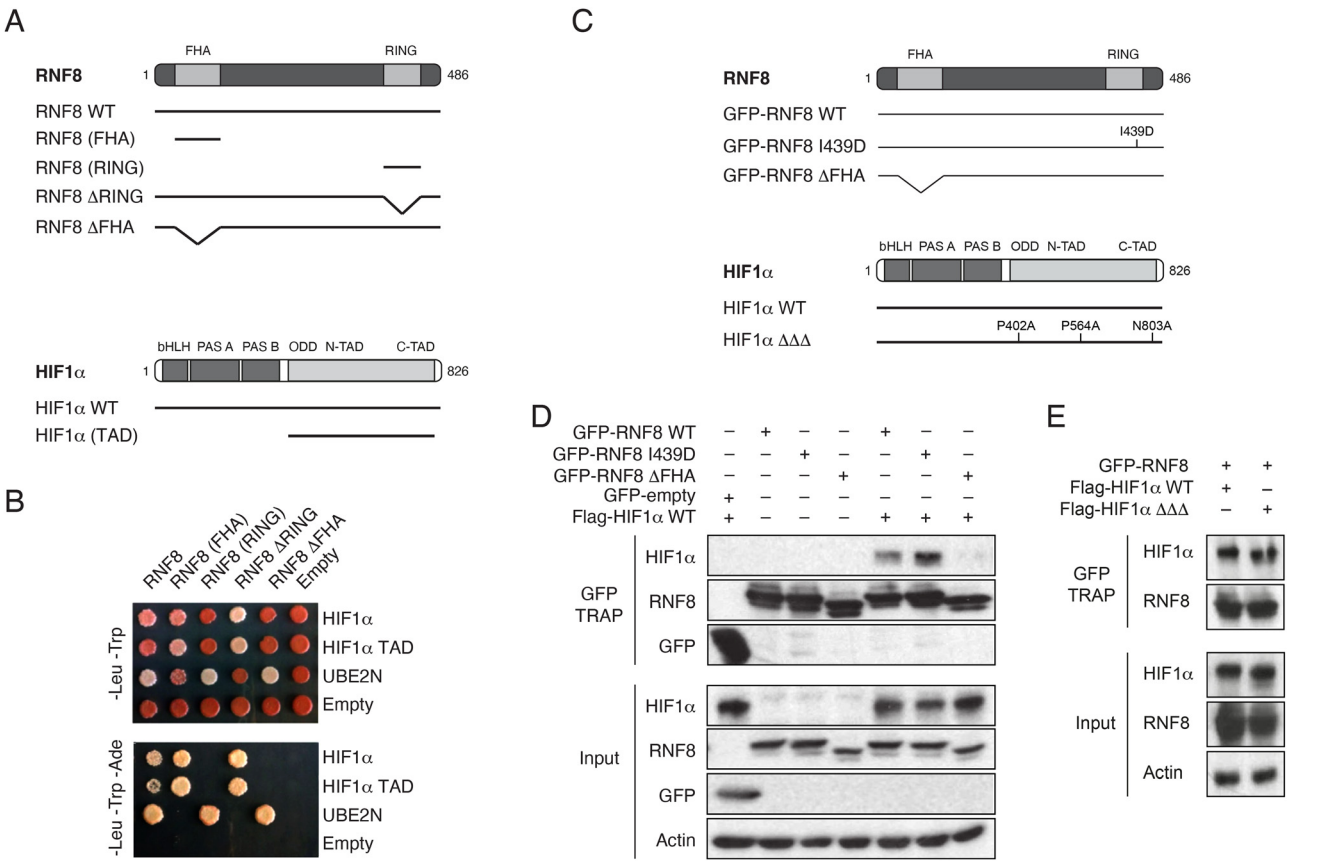

Fig. 2 RNF8 binds the C-terminal TAD domain of HIF1α *via* its FHA domain in a hydroxylation-independent manner. (A) Domain mapping using Y2H with truncation constructs of RNF8 and HIF1α. (B) Interaction requires the RNF8 FHA domain and the HIF1α TAD domain. (C) Domain mapping using truncation/mutant constructs of RNF8 and HIF1α. (D) Co-IP of GFP-HIF1α WT with different Flag-RNF8 mutants in HEK293T cells. Interaction requires FHA but not RING domain. (E) Co-IP of GFP-RNF8 with HIF1α WT or the hydroxylation-resistant HIF1α ΔΔΔ mutant. Interaction is maintained independently of HIF1α hydroxylation status.

motif. Future studies will elaborate whether this site within HIF1α is critical for binding to the RNF8-FHA domain.

Interestingly, structural and functional studies have shown that the FHA domain of RNF8 can also mediate phospho-independent interactions. For example, RNF8 was found to recruit the chromatin remodeling factor CHD4 *via* a non-canonical, phospho-independent interface within its FHA domain.[29] This evidence is supported by the fact that the FHA domain of RNF8 has structural features likely mediating phospho-independent interactions.[2,26,29] This suggests that the RNF8 FHA domain may possess a more versatile interaction surface than previously appreciated and HIF1α could represent an additional binding partner that exploits this non-canonical binding property of the FHA domain.

As mentioned above, HIF1α is constitutively expressed but rapidly degraded under normoxic conditions due to post-translational modifications mediated by prolyl-4-hydroxylases (PHDs). Hydroxylated HIF1α is subsequently recognized and ubiquitinated by the E3 ligase VHL, targeting it for proteasomal degradation.[30–32] To investigate whether the interaction between RNF8 and HIF1α is also dependent on oxygen condition, similar to the VHL-HIF1α interaction, we generated a hydroxylation-resistant HIF1α mutant by introducing three point mutations in its C-terminal transactivation domain (P402A, P564A, and N803A). This stabilized form of HIF1α (hereafter referred to as HIF1α ΔΔΔ) is not hydroxylated and thus escapes VHL-mediated degradation. GFP-Trap pulldown experiments demonstrated that GFP-RNF8 WT interacts with both Flag-HIF1α WT and Flag-HIF1α ΔΔΔ, showing that the interaction is independent of HIF1α hydroxylation (Fig. 2E). Notably, VHL does not interact with HIF1α in *S. cerevisiae*,[33] whereas RNF8 does (see this study), further supporting the notion that the RNF8-HIF1α interaction is independent of hydroxylation and might preferentially take place under hypoxic conditions. To determine whether the FHA-TAD association reflects a direct interaction between purified components, we performed biochemical binding assays using bacterially expressed GST-tagged RNF8 FHA domain and a His-tagged HIF1α fragment spanning amino acids 1 to 735 aa. However, biochemical AlphaScreen-based interaction analysis did not detect a robust interaction under the tested conditions (data not shown). These findings suggest that the RNF8-HIF1α interaction may either require post-translational modifications, or a conformational context not recapitulated in the minimal biochemical system or additional cellular factors. Future studies will explore the exact nature of this interaction.

RNF8 counteracts TRAF6-mediated stabilization of HIF1α in cells

In line with a previous observation,[15] we found that TRAF6 stabilizes and co-precipitates with HIF1α (Fig. 3A). Interestingly, TRAF6 also co-immunoprecipitated with RNF8 (Fig. 3B). RNF8 protein levels also appear to be stabilized upon TRAF6 overexpression (Fig. 3B). These data indicated that not only HIF1α interacts with RNF8 and TRAF6, respectively, but also RNF8 and TRAF6 interact among each other. This interaction is most likely not bridged *via* HIF1α, since we detected it also under normoxic conditions. However, we cannot rule out that this interaction is bridged by other proteins.

To gain insight into the interplay between RNF8, TRAF6, and HIF1α under normoxic and hypoxia-mimetic conditions, cells were co-transfected with the indicated constructs, treated with $CoCl_2$, and analyzed by immunoblotting of whole-cell lysates and GFP-based pull-downs (Fig. 3C). In whole-cell lysates, co-expression of TRAF6 led to detectable HIF1α levels already under normoxic conditions, consistent with previous reports showing that TRAF6 stabilizes HIF1α. Upon $CoCl_2$ treatment, HIF1α levels further increased, indicating additional stabilization under hypoxia-mimetic conditions. In contrast, co-expression of GFP-RNF8 markedly reduced HIF1α protein levels under both normoxic and hypoxic conditions.

Analysis of the corresponding GFP-RNF8 pull-downs from the same experiment revealed that both HIF1α and TRAF6 associated with RNF8. Notably, $CoCl_2$ treatment resulted in a pronounced reduction of TRAF6 co-precipitation with RNF8, whereas the interaction between RNF8 and HIF1α was maintained. Importantly, total TRAF6 levels in the input were unchanged, indicating that the reduced recovery of TRAF6 reflects altered binding rather than decreased protein abundance. Although overall HIF1α levels in the lysate were strongly reduced in the presence of RNF8, HIF1α remained readily detectable in RNF8 pull-downs, consistent with a model in which RNF8 efficiently engages HIF1α in a transient, turnover-associated interaction that precedes HIF1α destabilization.

Together, these observations suggest that RNF8 associates with HIF1α in a manner that is closely linked to HIF1α destabilization. They further support an antagonistic, potentially competitive relationship between RNF8 and TRAF6 in the regulation of HIF1α under hypoxia-mimetic conditions.

To determine whether the effect on HIF1α turnover depends on the E3 ligase activity of RNF8, we overexpressed RNF8 wild type (WT), RNF8 lacking the FHA domain (ΔFHA), or RNF8 lacking the RING domain (ΔRING), together with HIF1α and TRAF6. Consistent with our previous results, co-expression of RNF8 WT with TRAF6 led to a strong reduction in HIF1α protein levels, regardless of $CoCl_2$ treatment (Fig. 3D). We did not observe this effect when RNF8 ΔFHA was expressed, indicating that the FHA domain is required. In contrast, RNF8 ΔRING behaved similarly to RNF8 WT and resulted in reduced HIF1α levels. These findings are consistent with the data in Fig. 2, showing that the FHA domain is crucial for the interaction between RNF8 and HIF1α. Together, these results suggest that the interaction of RNF8 with HIF1α *via* its FHA domain modulates HIF1α protein levels in the presence of TRAF6, while the E3 ligase activity of RNF8 is dispensable for this effect.

Next, we investigated whether RNF8 localizes to the nucleus under hypoxic conditions in a triple-negative breast cancer context and whether this localization is functionally linked to HIF1α regulation. Using MDA-MB-231 cells, a well-established TNBC model, subcellular fractionation assays performed in the presence or absence of the hypoxia-mimetic $CoCl_2$ and in combination with siRNA-mediated RNF8 depletion revealed

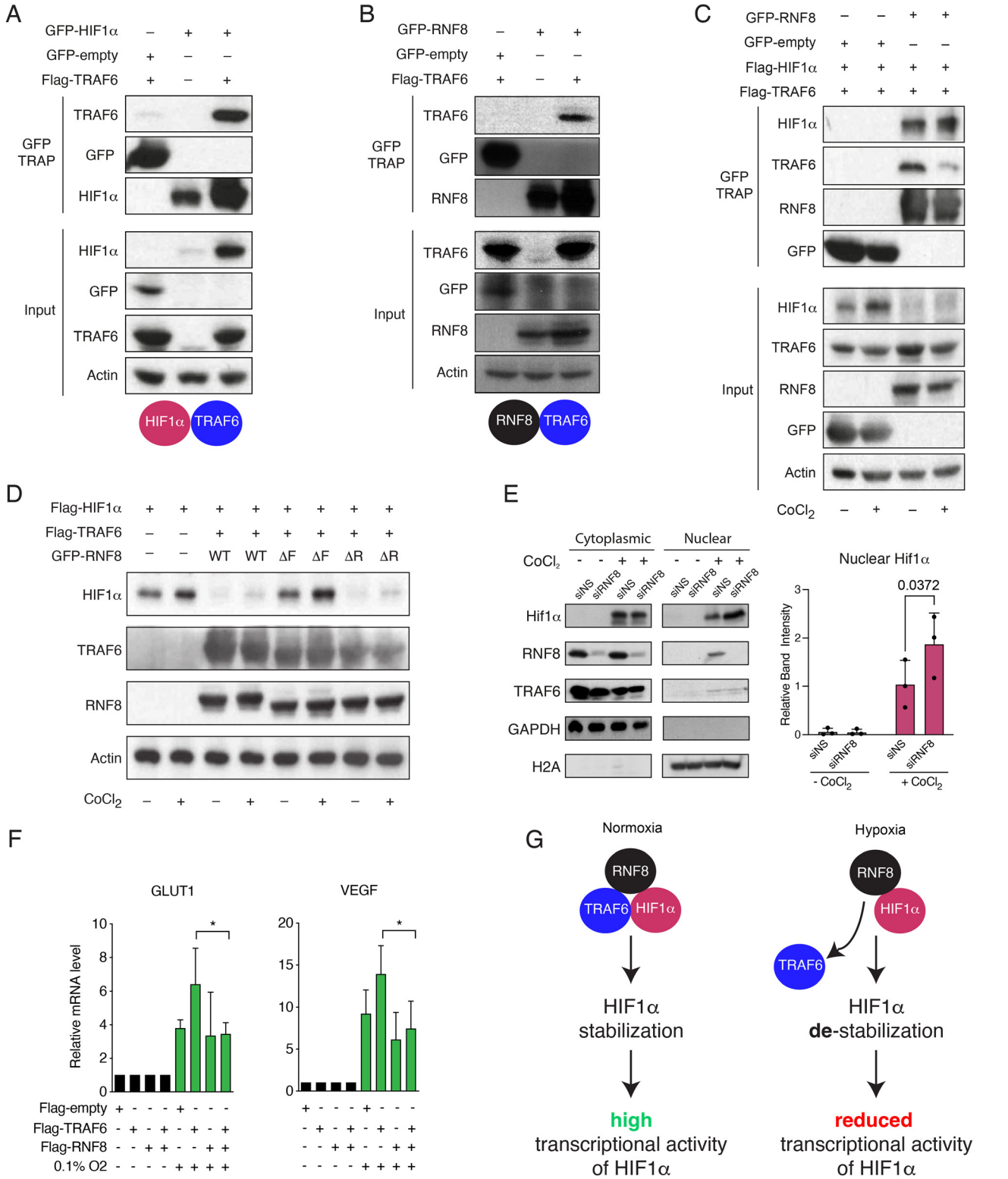

Fig. 3 RNF8 counteracts TRAF6-mediated HIF1α stabilization and transcriptional activity under hypoxic conditions. (A) Co-immunoprecipitation (co-IP) of Flag-HIF1α with GFP-TRAF6 in HEK293T cells. (B) Co-IP of GFP-RNF8 with Flag-TRAF6 in HEK293T cells. (C) Whole-cell lysates (input) expressing HIF1α and TRAF6 with or without GFP-RNF8 under normoxia or $CoCl_2$ treatment (hypoxia mimic), and GFP-RNF8 pull-downs, were analyzed by immunoblotting for HIF1α and TRAF6 levels. (D) Analysis of HIF1α protein levels upon co-expression with RNF8 WT, RNF8 ΔFHA, or RNF8 ΔRING in the presence of TRAF6 under normoxia or $CoCl_2$ treatment (hypoxia mimic). (E) Left: MDA-MB-231 cells were transfected with control or RNF8-targeting siRNA and treated with the hypoxia-mimetic $CoCl_2$ as indicated. Cytoplasmic and nuclear fractions were prepared and analyzed by immunoblotting (representative blots from one of three independent experiments) for RNF8 and HIF1α. H2A and GAPDH were used as nuclear and cytoplasmic markers, respectively. Right: densitometric quantification of nuclear HIF1α normalized to H2A, from three independent experiments (n = 3). (F) qRT-PCR of HIF1α target genes *VEGF* and *Glut1* in MDA-MB-231 cells upon overexpression of RNF8 and TRAF6 under normoxic or hypoxic (0.1% O_2) conditions. (G) Schematic model: TRAF6 stabilizes HIF1α to drive hypoxia-responsive transcription. Conversely, RNF8 binds HIF1α *via* its FHA domain to counteract this process. Independent of E3 ligase activity, RNF8 interferes with the TRAF6-HIF1α complex, reducing nuclear HIF1α accumulation and transcriptional output.

that RNF8 translocates to the nucleus under hypoxia-like conditions (Fig. 3E). Importantly, RNF8 knockdown resulted in a pronounced increase in nuclear HIF1α levels under hypoxia-mimetic conditions (Fig. 3E, left; quantified in the right panel), whereas cytoplasmic HIF1α levels were largely unaffected (Fig. 3E). Given that HIF1α functions as a nuclear transcription factor, these data provide physiological evidence that endogenous RNF8 limits nuclear HIF1α accumulation during hypoxic signaling. Previous studies have shown that hypoxia triggers nuclear stress responses without inducing classical DNA damage repair pathways that involve RNF8.[34] Supporting this, later work showed that RNF8 and MDC1 are not required for H2AX-mediated stabilization of HIF1α in hypoxic cells,[35] suggesting that RNF8 is not part of the canonical TRAF6–ATM–H2AX signaling axis in this context. Instead, our data support a model in which RNF8 acts as a context-dependent nuclear modulator of HIF1α. The hypoxia-induced nuclear presence of RNF8, together with the increased nuclear accumulation of HIF1α upon RNF8 depletion, suggests that RNF8 fine-tunes hypoxic signaling by promoting turnover of nuclear HIF1α or associated regulatory complexes rather than acting as a core component of hypoxia-driven transcription.

Finally, we analyzed the mRNA levels of the HIF1α target genes *VEGF* and *Glut1* in MDA-MB-231 cells upon overexpression of TRAF6, RNF8, or both in combination. As expected, TRAF6 overexpression led to increased expression of *VEGF* and *Glut1* under hypoxic conditions (0.1% O_2) compared to the control. Notably, co-expression of RNF8 significantly reduced the expression levels of both target genes (Fig. 3F). These results suggest that the RNF8-mediated reduction in HIF1α protein levels in the presence of TRAF6 has functional consequences at the transcriptional level, supporting the notion that RNF8 negatively modulates HIF1α activity under hypoxic conditions. Given that this effect occurs despite the presence of TRAF6, which typically enhances HIF1α stability and activity, RNF8 appears to exert a dominant inhibitory effect in this context. Whether this inhibition is solely due to reduced HIF1α protein levels or also involves interference with transcriptional co-activator recruitment remains to be determined. However, the data clearly show that RNF8 modulates not only HIF1α protein abundance but also its downstream transcriptional output.

Our findings support a model in which RNF8 acts in a non-catalytic manner to limit nuclear HIF1α stabilization and transcriptional activity under hypoxic conditions, likely through a scaffolding or competitive mechanism involving both HIF1α and TRAF6 (Fig. 3G). Previous studies revealed that TRAF6 enhances HIF1α protein stability and transcriptional output under both normoxic and hypoxic conditions. However, the precise mechanism, whether *via* direct ubiquitination, stabilization of protein complexes, or alternative signaling pathways, remains incompletely understood.

Consistent with an antagonistic relationship, co-expression of RNF8 with TRAF6 resulted in a marked reduction of HIF1α protein levels in whole-cell lysates, even in the presence of hypoxia mimetics such as $CoCl_2$. This observation indicates that RNF8 counteracts TRAF6-mediated HIF1α stabilization at the level of protein abundance. In parallel, GFP-RNF8 pull-down experiments revealed robust association of RNF8 with HIF1α, despite strongly reduced total HIF1α levels, suggesting that RNF8 engages a functionally relevant HIF1α pool that is coupled to subsequent destabilization.

We further show that RNF8 interacts with both HIF1α and TRAF6, and this interaction critically depends on the FHA domain but not the RING domain, indicating that RNF8 exerts its negative regulatory function independently of its E3 ubiquitin ligase activity.

Notably, siRNA-mediated depletion of endogenous RNF8 led to increased accumulation of HIF1α specifically in the nuclear fraction under hypoxia-mimetic conditions, providing physiological evidence that RNF8 restrains nuclear HIF1α levels. The hypoxia-induced nuclear localization of RNF8 provides a spatial framework for this regulation. Functionally, this antagonistic interaction is reflected by reduced expression of HIF1α target genes such as VEGF and GLUT1 upon RNF8 expression, even in the presence of TRAF6 and hypoxic stimulation. Both, TRAF6 and HIF1α, have been implicated in promoting glycolysis, chemoresistance, and tumor progression in triple-negative breast cancer (TNBC). The ability of RNF8 to counteract TRAF6-mediated stabilization of HIF1α and suppress hypoxia-induced transcriptional programs; thus, represents a previously unrecognized regulatory axis relevant to aggressive tumor biology.

Conclusion

In summary, these findings highlight a non-canonical inhibitory role of RNF8 in the regulation of HIF1α abundance and activity. This suggests a broader function of RNF8 in modulating cellular responses to hypoxia. Independent of its ubiquitin ligase activity, RNF8 forms a complex with both HIF1α and TRAF6 *via* its FHA domain and limits HIF1α protein stabilization and transcriptional output under hypoxic conditions. Consistent with this notion, RNF8 localizes to the nucleus under hypoxia and restrains nuclear accumulation of HIF1α, thereby attenuating the expression of key HIF1α target genes. Together, our results suggest that RNF8 may serve as a fine-tuner of cellular adaptation to low oxygen. Further studies will explore the physiological relevance of this mechanism *in vivo* and its potential implications in cancer pathologies such as in TNBC.

Author contributions

KS and KH conceptualized this study, LR and EMW applied the methods, performed experiments and analyzed the data, KS and KH supervised the work, KH acquired funding, LR, KS and KH wrote the original draft; All authors reviewed and edited the manuscript.

Conflicts of interest

K. H. is inventor on patents involving the E3 ligase TRAF6 (WO/2018/050286 and WO/2019/180207).

Data availability

All data are available in the article and its supplementary information (SI). The data supporting this article have been included as part of the SI. Supplementary information is available. See DOI: https://doi.org/10.1039/d5cb00209e.

Acknowledgements

Funded in part by the Deutsche Forschungsgemeinschaft (DFG, German Research Foundation) – TRR 387/1 – 514894665. Artificial intelligence (AI) tools including ChatGPT and DeepL were employed in this manuscript to refine grammar, spelling, and readability. These tools were used exclusively for linguistic enhancement without altering the scientific content, interpretation, or conclusions. All intellectual contributions, data analyses, and critical discussions remain the work of the authors. The final manuscript was thoroughly reviewed and approved by all co-authors to ensure accuracy and integrity.

Notes and references

1 T. Thorslund, A. Ripplinger, S. Hoffmann, T. Wild, M. Uckelmann, B. Villumsen, T. Narita, T. K. Sixma, C. Choudhary, S. Bekker-Jensen and N. Mailand, *Nature*, 2015, **527**, 389–393.
2 M. S. Huen, R. Grant, I. Manke, K. Minn, X. Yu, M. B. Yaffe and J. Chen, *Cell*, 2007, **131**, 901–914.
3 F. Mattiroli, J. H. Vissers, W. J. van Dijk, P. Ikpa, E. Citterio, W. Vermeulen, J. A. Marteijn and T. K. Sixma, *Cell*, 2012, **150**, 1182–1195.
4 S. J. Campbell, R. A. Edwards, C. C. Leung, D. Neculai, C. D. Hodge, S. Dhe-Paganon and J. N. Glover, *J. Biol. Chem.*, 2012, **287**, 23900–23910.
5 P. Valnegri, J. Huang, T. Yamada, Y. Yang, L. A. Mejia, H. Y. Cho, A. Oldenborg and A. Bonni, *Nat. Commun.*, 2017, **8**, 1271.
6 W. M. Baarends, J. W. Hoogerbrugge, H. P. Roest, M. Ooms, J. Vreeburg, J. H. Hoeijmakers and J. A. Grootegoed, *Dev. Biol.*, 1999, **207**, 322–333.
7 R. Rai, J. M. Li, H. Zheng, G. T. Lok, Y. Deng, M. S. Huen, J. Chen, J. Jin and S. Chang, *Nat. Struct. Mol. Biol.*, 2011, **18**, 1400–1407.
8 H. J. Lee, C. F. Li, D. Ruan, S. Powers, P. A. Thompson, M. A. Frohman and C. H. Chan, *Mol. Cell*, 2016, **63**, 1021–1033.
9 W. G. Kaelin, Jr. and P. J. Ratcliffe, *Mol. Cell*, 2008, **30**, 393–402.
10 P. H. Maxwell, M. S. Wiesener, G. W. Chang, S. C. Clifford, E. C. Vaux, M. E. Cockman, C. C. Wykoff, C. W. Pugh, E. R. Maher and P. J. Ratcliffe, *Nature*, 1999, **399**, 271–275.
11 C. Chen, N. Pore, A. Behrooz, F. Ismail-Beigi and A. Maity, *J. Biol. Chem.*, 2001, **276**, 9519–9525.
12 P. Chaturvedi, D. M. Gilkes, N. Takano and G. L. Semenza, *Proc. Natl. Acad. Sci. U. S. A.*, 2014, **111**, E2120–2129.
13 Cancer Genome Atlas Network, *Nature*, 2012, **490**, 61–70.
14 J. Tutzauer, M. Sjöström, E. Holmberg, P. Karlsson, F. Killander, L. M. F. Leeb-Lundberg, P. Malmström, E. Niméus, M. Fernö and A. Jögi, *Br. J. Cancer*, 2022, **126**, 1145–1156.
15 H. Sun, X. B. Li, Y. Meng, L. Fan, M. Li and J. Fang, *Cancer Res.*, 2013, **73**, 4950–4959.
16 J. Liu, C. Zhang, Y. Zhao, X. Yue, H. Wu, S. Huang, J. Chen, K. Tomsky, H. Xie, C. A. Khella, M. L. Gatza, D. Xia, J. Gao, E. White, B. G. Haffty, W. Hu and Z. Feng, *Nat. Commun.*, 2017, **8**, 1823.
17 A. Falconieri, G. Minervini, R. Bortolotto, D. Piovesan, R. Lopreiato, G. Sartori, M. Pennuto and S. C. E. Tosatto, *Sci. Rep.*, 2020, **10**, 15850.
18 K. Nakayama, I. J. Frew, M. Hagensen, M. Skals, H. Habelhah, A. Bhoumik, T. Kadoya, H. Erdjument-Bromage, P. Tempst, P. B. Frappell, D. D. Bowtell and Z. Ronai, *Cell*, 2004, **117**, 941–952.
19 E. Scharschmidt, E. Wegener, V. Heissmeyer, A. Rao and D. Krappmann, *Mol. Cell. Biol.*, 2004, **24**, 3860–3873.
20 S. Bekker-Jensen, J. Rendtlew Danielsen, K. Fugger, I. Gromova, A. Nerstedt, C. Lukas, J. Bartek, J. Lukas and N. Mailand, *Nat. Cell Biol.*, 2010, **12**, 80–86; sup pp. 81–12.
21 G. Markson, C. Kiel, R. Hyde, S. Brown, P. Charalabous, A. Bremm, J. Semple, J. Woodsmith, S. Duley, K. Salehi-Ashtiani, M. Vidal, D. Komander, L. Serrano, P. Lehner and C. M. Sanderson, *Genome Res.*, 2009, **19**, 1905–1911.
22 K. Luck, D. K. Kim, L. Lambourne, K. Spirohn, B. E. Begg, W. Bian, R. Brignall, T. Cafarelli, F. J. Campos-Laborie, B. Charloteaux, D. Choi, A. G. Coté, M. Daley, S. Deimling, A. Desbuleux, A. Dricot, M. Gebbia, M. F. Hardy, N. Kishore, J. J. Knapp, I. A. Kovács, I. Lemmens, M. W. Mee, J. C. Mellor, C. Pollis, C. Pons, A. D. Richardson, S. Schlabach, B. Teeking, A. Yadav, M. Babor, D. Balcha, O. Basha, C. Bowman-Colin, S. F. Chin, S. G. Choi, C. Colabella, G. Coppin, C. D'Amata, D. De Ridder, S. De Rouck, M. Duran-Frigola, H. Ennajdaoui, F. Goebels, L. Goehring, A. Gopal, G. Haddad, E. Hatchi, M. Helmy, Y. Jacob, Y. Kassa, S. Landini, R. Li, N. van Lieshout, A. MacWilliams, D. Markey, J. N. Paulson, S. Rangarajan, J. Rasla, A. Rayhan, T. Rolland, A. San-Miguel, Y. Shen, D. Sheykhkarimli, G. M. Sheynkman, E. Simonovsky, M. Taş an, A. Tejeda, V. Tropepe, J. C. Twizere, Y. Wang, R. J. Weatheritt, J. Weile, Y. Xia, X. Yang, E. Yeger-Lotem, Q. Zhong, P. Aloy, G. D. Bader, J. De Las Rivas, S. Gaudet, T. Hao, J. Rak, J. Tavernier, D. E. Hill, M. Vidal, F. P. Roth and M. A. Calderwood, *Nature*, 2020, **580**, 402–408.
23 C. Liu, J. Kuang, Y. Wang, T. Duan, L. Min, C. Lu, T. Zhang, R. Chen, Y. Wu and L. Zhu, *Biol. Direct*, 2022, **17**, 17.
24 Y. H. Chuah, E. X. Y. Tay, O. V. Grinchuk, J. Yoon, J. Feng, S. Kannan, M. Robert, R. Jakhar, Y. Liang, B. W. L. Lee, L. C. Wang, Y. T. Lim, T. Zhao, R. M. Sobota, G. Lu, B. C. Low, K. C. Crasta, C. S. Verma, Z. Lin and D. S. T. Ong, *Cell Death Differ.*, 2023, **30**, 1973–1987.
25 D. Durocher, J. Henckel, A. R. Fersht and S. P. Jackson, *Mol. Cell*, 1999, **4**, 387–394.

26 D. Durocher, I. A. Taylor, D. Sarbassova, L. F. Haire, S. L. Westcott, S. P. Jackson, S. J. Smerdon and M. B. Yaffe, *Mol. Cell*, 2000, **6**, 1169–1182.
27 J. Li, G. I. Lee, S. R. Van Doren and J. C. Walker, *J. Cell Sci.*, 2000, **113 Pt 23**, 4143–4149.
28 K. Gradin, C. Takasaki, Y. Fujii-Kuriyama and K. Sogawa, *J. Biol. Chem.*, 2002, **277**, 23508–23514.
29 M. S. Luijsterburg, K. Acs, L. Ackermann, W. W. Wiegant, S. Bekker-Jensen, D. H. Larsen, K. K. Khanna, H. van Attikum, N. Mailand and N. P. Dantuma, *EMBO J.*, 2012, **31**, 2511–2527.
30 L. E. Huang, J. Gu, M. Schau and H. F. Bunn, *Proc. Natl. Acad. Sci. U. S. A.*, 1998, **95**, 7987–7992.
31 J. F. O'Rourke, Y. M. Tian, P. J. Ratcliffe and C. W. Pugh, *J. Biol. Chem.*, 1999, **274**, 2060–2071.
32 K. Tanimoto, Y. Makino, T. Pereira and L. Poellinger, *EMBO J.*, 2000, **19**, 4298–4309.
33 C. Bex, K. Knauth, S. Dambacher and A. Buchberger, *Nucleic Acids Res.*, 2007, **35**, e142.
34 Z. Bencokova, M. R. Kaufmann, I. M. Pires, P. S. Lecane, A. J. Giaccia and E. M. Hammond, *Mol. Cell. Biol.*, 2009, **29**, 526–537.
35 A. H. Rezaeian, C. F. Li, C. Y. Wu, X. Zhang, J. Delacerda, M. J. You, F. Han, Z. Cai, Y. S. Jeong, G. Jin, L. Phan, P. C. Chou, M. H. Lee, M. C. Hung, D. Sarbassov and H. K. Lin, *Nat. Cell Biol.*, 2017, **19**, 38–51.